

Machine learning bridges microslips and slip avalanches of sheared granular gouge

Gang Ma¹, Jiangzhou Mei¹, Ke Gao², Jidong Zhao³, Wei Zhou⁴, and Di Wang¹

¹Wuhan University

²Southern University of Science and Technology

³Hong Kong University of Science and Technology

⁴State Key Laboratory of Water Resources and Hydropower Engineering Science, Wuhan University

November 26, 2022

Abstract

Understanding the origin of stress avalanche of fault gouges may offer deeper insights into many geophysical processes such as earthquakes. Microslips of sheared granular gouges were found to be precursors of large slip events, but the documented relation between local and global avalanches remains largely qualitative. We examine the stick-slip behavior of a slowly sheared granular system using discrete element method simulations. The microslips, i.e., local avalanche events, are found to demonstrate significantly different statistical and spatial characteristics between the stick and slip states. We further investigate the correlation between the global stress fluctuations and the features extracted from microslips based on the machine learning (ML) approach. The data-driven model that incorporates the information of the spatial distribution of microslips can robustly predict the magnitude of stress fluctuation. A further feature importance analysis confirms that the spatial patterns of microslips manifest key information governing the global stress fluctuations.

Hosted file

supporting information.doc available at <https://authorea.com/users/550468/articles/606372-machine-learning-bridges-microslips-and-slip-avalanches-of-sheared-granular-gouge>

1 **Machine learning bridges microslips and slip avalanches of sheared granular gouge**

2
3 **Gang Ma^{1,2}, Jiangzhou Mei^{1,2}, Ke Gao³, Jidong Zhao⁴, Wei Zhou^{1,2}, Di Wang^{1,2}**

4
5 ¹ State Key Laboratory of Water Resources and Hydropower Engineering Science, Wuhan
6 University, Wuhan 430072, China.

7 ² Key Laboratory of Rock Mechanics in Hydraulic Structural Engineering of Ministry of
8 Education, Wuhan University, Wuhan 430072, China.

9 ³ Department of Earth and Space Sciences, Southern University of Science and Technology,
10 Shenzhen 518055, Guangdong, China.

11 ⁴ Department of Civil and Environmental Engineering, The Hong Kong University of Science
12 and Technology, Clear Water Bay, Kowloon, Hong Kong, China

13
14 Corresponding author: Jiangzhou Mei (whu_meijz@whu.edu.cn)

15
16 **Key Points:**

- 17 • The microslips of sheared granular gouge demonstrate different statistical and spatial
18 characteristics in stick and slip states
- 19 • Clustering of large microslips is correlated closely to large stress drop
- 20 • Machine learning establish a quantitative relationship between microslips and global
21 stress fluctuations

22
23

24 **Abstract**

25 Understanding the origin of stress avalanche of fault gouges may offer deeper insights into many
26 geophysical processes such as earthquakes. Microslips of sheared granular gouges were found to
27 be precursors of large slip events, but the documented relation between local and global
28 avalanches remains largely qualitative. We examine the stick-slip behavior of a slowly sheared
29 granular system using discrete element method simulations. The microslips, i.e., local avalanche
30 events, are found to demonstrate significantly different statistical and spatial characteristics
31 between the stick and slip states. We further investigate the correlation between the global stress
32 fluctuations and the features extracted from microslips based on the machine learning (ML)
33 approach. The data-driven model that incorporates the information of the spatial distribution of
34 microslips can robustly predict the magnitude of stress fluctuation. A further feature importance
35 analysis confirms that the spatial patterns of microslips manifest key information governing the
36 global stress fluctuations.

37

38 **Plain Language Summary**

39 Frictional instability of natural fault gouges may play a key role in numerous geophysical
40 processes, such as earthquakes and debris flows. Direct investigation of natural faults is difficult
41 owing to their burial depth and broad distribution beneath the earth. Structural and statistical
42 similarities between granular materials and fault gouges render the former an ideal model system
43 for understanding the mechanism of natural fault gouges. When slowly deformed, granular
44 materials generate cycles of friction increase and reduction, i.e., stick-slip cycles, analogous to
45 the earthquake cycles. Microslips are found to be precursors of large slip events, but their
46 correlations are mostly qualitative. This study uses numerical simulations to generate a series of
47 stick-slip cycles of slowly sheared granular gouge. Distinctive differences are observed in the
48 statistical and spatial characteristics of microslips between stick and slip stages. A trained
49 machine learning model is further used to predict the global slip avalanche from the features
50 extracted from microslips and its prediction accuracy can be significantly improved when
51 considering the spatial information of microslips. This work suggests that the microslips detected
52 inside natural gouge faults (e.g., local acoustic emission signal or local seismic wave) and their
53 locations can be used to assess their frictional stability.

54

55 **1 Introduction**

56 The frictional stability of fault gouge layers underpins key understandings to many geophysical
57 processes, including but not limited to earthquakes, debris flows, and landslides (Song et al.,
58 2017; Ren et al., 2019; Nanjo, 2020). A granular gouge subjected to slow shearing demonstrates
59 a typical stick-slip behavior, which plays a crucial role in triggering the frictional stability of the
60 fault (Byerlee & Brace, 1966; Marone et al., 1991; Aharonov & Sparks, 2004; Denisov et al.,
61 2016; Dorostkar & Carmeliet, 2019). Therefore, the stick-slip behavior of sheared granular
62 gouges has been studied extensively in both laboratory experiments (Marone, 1998; Niemeijer et
63 al., 2010; Scuderi et al., 2015, 2016; Leeman et al., 2016; Tinti et al., 2016; Rivière et al., 2018)
64 and numerical simulations (Aharonov & Sparks, 2004; Mair & Hazzard, 2007; Ferdowsi et al.,
65 2014b; Dorostkar et al., 2017a; Gao et al., 2018; Ma et al., 2020). Particular attention has been
66 placed on the influences of controlling factors on the stick-slip dynamics of granular gouge, such

67 as the wall geometry and friction (Rathbun et al., 2013), presence of liquids (Dorostkar et al.,
68 2017b, 2018), particle characteristics (Mair et al., 2002; Dorostkar & Carmeliet, 2019), boundary
69 vibration (Ferdowsi et al., 2014a), normal pressure (Gao et al., 2018), particle size polydispersity
70 (Ma et al., 2020), and particle breakage (Wang et al., 2020). These studies offer novel insights
71 into the complex dynamic behaviors of natural fault gouges and earthquake physics.

72

73 However, the microscopic origin of slip avalanche of slowly deformed granular gouge remains
74 poorly understood. To address this issue, Johnson et al. (2013) employed a biaxial shear
75 apparatus to investigate the physics of laboratory earthquake and found that the acoustic
76 emission and microslip exhibit an exponential increase in the rate of occurrence, reaching a peak
77 at the onset of slip avalanche. The corresponding DEM simulations confirmed that the microslip
78 event rate correlates well with large slip event onset (Ferdowsi et al., 2013). Microslip or local
79 avalanche is essentially a result of the localized particle rearrangements (Ma et al., 2021). Due to
80 the disordered structure of granular materials, a microslip may trigger nearby microslips, and the
81 accumulation of these microslips may give rise to a global stress avalanche (Castellanos &
82 Zaiser, 2018; Cao et al., 2019). Thus, microslips are widely regarded as precursors of large slip
83 events and can be used to predict frictional weakening (Bolton et al., 2019, 2020; Trugman et al.,
84 2020).

85

86 Furthermore, the statistics of local and global avalanches reveal a simple relation between the
87 number of local avalanches and the global avalanches (Barés et al., 2017). The spatial
88 characteristics of microslips are also closely correlated with the stress avalanche, where large
89 stress drop is accompanied by a series of connected localized zones spanning the entire system,
90 whereas during the elastic regime, the microslip events occur with low concentration and are
91 spatially dispersed (Cao et al., 2018). Other particle scale metrics, such as coordination number,
92 sliding contact ratio, potential energy, kinetic energy, evolves correspondingly during the stick
93 phase and slip instability (Ferdowsi et al., 2015; Barés et al., 2017; Dorostkar & Carmeliet, 2018;
94 Ma et al., 2020). Thus, studying the microscopic structure and dynamics of a granular gouge may
95 help to unveil its stick-slip behaviors (Cipelletti et al., 2019).

96

97 Unfortunately, existing findings on the relation between microslips and global stress avalanche
98 remains largely qualitative, whereas further advance on the subject matter demands quantitative
99 correlations to be established. In this letter, we employ the machine learning (ML) approach to
100 bridge the microslips and global stress fluctuations, including both stress recharge (stick regime)
101 and stress drop (slip regime). ML offers data-driven approaches to automatically investigate the
102 underlying relations between variables and facilitate the process of revealing complex and
103 inexplicit patterns of large datasets (Marone, 2018; Bergen et al., 2019; Ren et al., 2020).
104 Particularly, ML has gained increasing popularity in recent years and has been widely used in
105 many areas of geoscience, such as predicting the timing and size of laboratory earthquakes
106 (Rouet-Leduc et al., 2017; Corbi et al., 2019), revealing the frictional state of granular fault
107 (Rouet-Leduc et al., 2018; Ren et al., 2019), estimating earthquake magnitude and GPS
108 displacement rate (Rouet-Leduc et al., 2019; Mousavi & Beroza, 2020), and performing
109 earthquake early warning and earthquake detection (Rouet-Leduc et al., 2018; Hulbert et al.,
110 2019; Mousavi et al., 2020; Trugman et al., 2020).

111

112 To do so, we perform the discrete element method (DEM) simulations of quasi-static shear of
113 granular gouge to achieve stick-slip dynamics. The microslip is manifested as the particle
114 rearrangements and quantified by the nonaffine particle motion. Then we compare between the
115 statistical and spatial characteristics of microslips in the stick and slip regimes. We use a two-
116 step scheme for feature selection to consider both the statistical and spatial characteristics of
117 microslips in the ML model training. The trained XGBoost model can well predict the global
118 stress fluctuation from the features extracted from the microslips. Finally, we analyze the feature
119 importance of the trained ML model and conclude that the spatial patterns of microslips contain
120 key information about the stick-slip dynamics of granular gouge.

121 2 Materials and Methods

122 DEM simulations of simple shear tests were performed to obtain data of microslips and global
123 stress fluctuations during the stick-slip cycles of granular gouge. Figure 1a shows the simple
124 shear model setup of the granular gouge, which consists of 9,134 particles with diameters
125 uniformly distributed from $0.8 d_{50}$ to $1.2 d_{50}$, where the average particle diameter $d_{50}=1.25$ mm.

126 The size of the granular gouge sample is $32 d_{50}$ (length) \times $16 d_{50}$ (depth) \times $16 d_{50}$ (height). The
127 granular gouge is confined by two rough particle walls used to apply the shear loading and
128 normal pressure. The top wall is fixed in the shear direction, while the normal pressure is
129 maintained constant by a servo-control at 10 MPa. The granular gouge is sheared by moving the
130 bottom wall in the x direction with a constant velocity while the vertical movement is
131 constrained. The shear rate $\dot{\gamma}$, defined as the ratio of shear velocity to the undeformed sample
132 height, is set to 0.05 to achieve stick-slip dynamics.

133

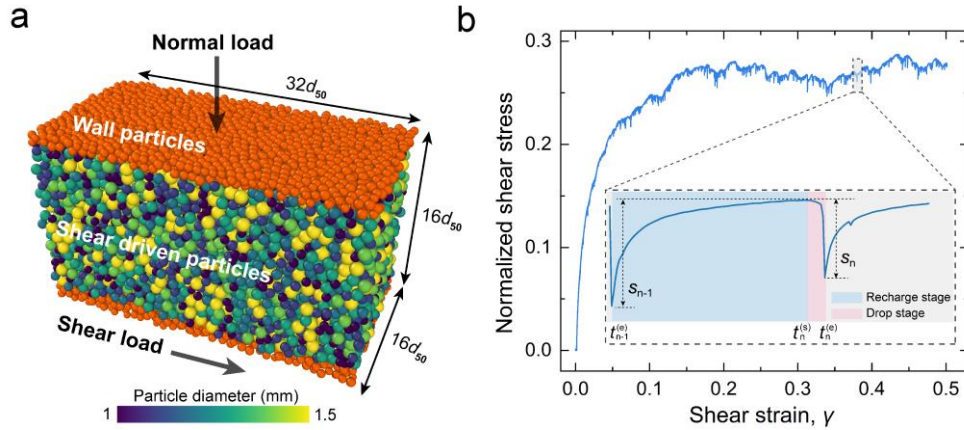
134 The numerical simulation is performed by the DEM code LIGGGHTS (Kloss et al., 2012). The
135 Hertz-Mindlin contact model with Coulomb sliding friction is employed to simulate the contacts
136 and deformation between particles. The particles have a density of 2900 kg/m^3 , a Poisson's ratio
137 of 0.25, Young's modulus of 65 GPa, a friction coefficient of 0.1, and a restitution coefficient of
138 0.87 (Ma et al., 2020). The wall particles adopt the same material properties as those in the shear
139 body. The friction coefficient between the particle walls and the shear body is set to 0.9 to
140 enhance surface friction. To collect enough data for the subsequent machine learning, we shear
141 the granular gouge up to a shear strain of 50%. The evolution of normalized shear stress, defined
142 as the ratio of shear stress σ to the applied normal pressure p , is shown in Figure 1b. When it is
143 sheared into the steady-state regime, the gouge is found to undergo typical intermittent dynamics
144 and serrated plastic flow. This phenomenon is seen to be universal in many amorphous solids
145 like metal glasses (Sun et al., 2012; Cao et al., 2018), and porous materials (Baró et al., 2013).

146

147 The enlarged view of the dotted box shown in Figure 1b demonstrates that each stick-slip cycle
148 starts with a nonlinear recharge of shear stress and is followed by a rapid drop. The recharge and
149 drop of shear stress correspond to the stick and slip stages, respectively. We define stress
150 fluctuation as the change of shear stress at the start and end of the recharge/drop events. Thus,
151 the stress fluctuation of a drop event is positive, and the recharge event negative. Only the

152 magnitude of stress fluctuation greater than a threshold of 10^{-5} is considered. During the slow
 153 shearing of granular gouge, we recorded 3,191 stress drop and recharge cycles.

154



155

156

157

158

159

160

161

162

163

164

165

166

167

168

169

170

171

172

173

174

175

176

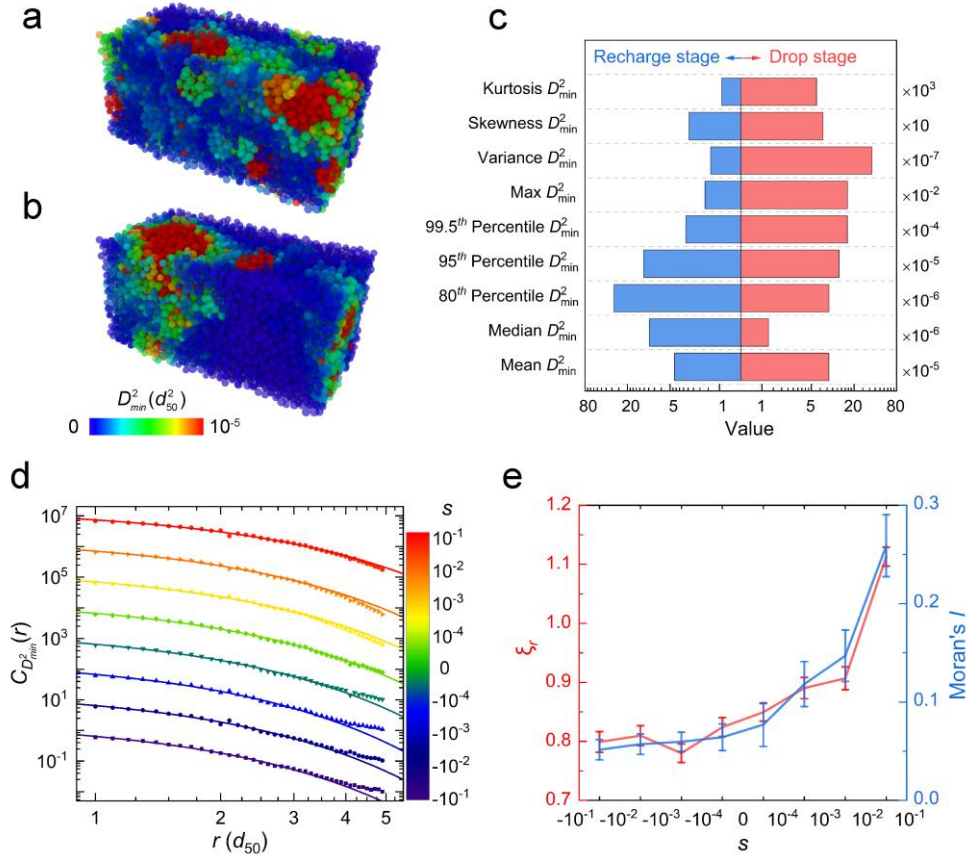
177

Figure 1. (a) Setup of the DEM experiment. Normal pressure and shear displacement are respectively applied on the top and bottom particle walls. Periodic boundary conditions are applied in the shear and depth directions. (b) Stress-strain curve resulted from the DEM simulation. The y axis denotes the shear stress σ normalized by the normal pressure p . The inset shows the enlarged stick-slip cycle which consists of stress recharge and drop stage represented by the blue and red shaded region, respectively.

3 Results

3.1 Statistical and spatial characteristics of microslips

The microslips that occurred during the recharge and drop events are manifested as irreversible particle rearrangements which are hereby quantified by the nonaffine particle displacements D_{\min}^2 (see Text S1) (Ma et al., 2021). It should be noted that many other quantities, such as local displacement, local energy fluctuation (Barés et al., 2017; Zheng et al., 2018), granular temperature (Ma et al., 2018, 2019), local acoustic emission (Trugman et al., 2020), force chain bulking (Gao et al., 2019; Liu et al., 2020) can also be used for characterizing microslips. Figure 2a and 2b show the spatial distributions of D_{\min}^2 during the recharge stage and the drop stage of a typical stick-slip cycle. Particles with higher D_{\min}^2 are colored in red. Due to the discrete nature and cooperative particle motion of granular materials, the deformation of granular gouge occurs as a succession of localized micro-slips distributed within the system. Intuitively, the microslips are scattered throughout the granular gouge during the recharge stage. During the drop stage, the microslips are more spatially concentrated and tend to establish large stress avalanches inside the granular gouge.



178 **Figure 2.** Statistical and spatial characteristics of microsliips occurred during recharge and drop stages. Spatial maps
 179 of D_{\min}^2 occurred during the (a) recharge state and (b) drop stage of a typical stick-slip cycle. (c) Comparison of the
 180 statistical quantities of D_{\min}^2 during the recharge and drop stage. (d) Normalized spatial correlation function of D_{\min}^2
 181 between two particles separated by distance r where r is in unit of the mean particle diameter. The data points are
 182 averaged over the recharge or drop stages falling into each bin. Solid lines are fits to the Ornstein-Zernike function.
 183 The data points and fitting lines of the different bin are shifted vertically for better visualization. (e) Evolutions of
 184 correlation length ξ_r and Moran' I with the magnitude of stress fluctuation. The error bar represents the standard
 185 deviation. Note that (d) and (e) are calculated over all stick-slip cycles.
 186

187
 188 Figure 2c compares the statistical features of microsliips that occurred during the recharge stage
 189 (blue) and drop stage (red) of a stick-slip cycle. The microsliips demonstrate significantly
 190 different statistical characteristics at the recharge stage and drop stage. For example, the 99.5th
 191 percentile, max, variance, skewness, and kurtosis are larger for drop stage. The difference in
 192 statistics of microsliips may suggest different underlying mechanism for stress recharge and stress
 193 drop. The stick-slip dynamics of granular materials can be seen as the jamming-unjamming
 194 process accompanied by the formation and buckling of force chains, which are triggered by
 195 localized particle rearrangements known as microsliips or local avalanches (Barés et al., 2017;
 196 Gao et al., 2019).

197
 198 The spatial distributions of microsliips that occurred during the recharge and drop stage can be
 199 further quantified using the normalized spatial correlation function (see Text S2) (Ma et al.,

200 2019, 2021). We group the recharge and drop events according to the magnitude and sign of
 201 stress fluctuation. Logarithmic binning is used. Figure 2d shows the normalized correlation
 202 functions $C_{D_{min}^2}(r)$ for recharge and drop events of different magnitudes. The spatial
 203 autocorrelation decays rapidly within a short distance of several d_{50} , showing a short-range
 204 ordering. Solid lines indicate that the decay of correlations with r are reasonably well fitted by
 205 the Ornstein-Zernike function as $C_{D_{min}^2}(r) \propto r^{-0.5} \exp(-r/\xi_r)$. We can see that the correlation
 206 length of microslips ξ_r remains nearly unchanged for recharge events and increases rapidly for
 207 large stress drop (see red line and left axis of Figure 2e). This trend indicates that a more
 208 cooperative and concentrated distribution of microslips constitutes the microscopic origin of
 209 global slip avalanche.

210

211 The spatial autocorrelation of microslips can also be quantified by global Moran's I (see Text
 212 S2) (Ma et al., 2019, 2021). The Moran's I of particle D_{min}^2 for recharge and drop events of
 213 different magnitudes show a very similar trend as the correlation length ξ_r (see blue line and
 214 right axis of Figure 2e). The spatial correlation analysis of microslips indicates that the spatially
 215 correlated microslips forming large shear transition zones are responsible for the stress drop and
 216 frictional weakening. The stress drop increases with the increasing degree of aggregation of
 217 microslips. The spatial distribution of microslips during recharge stages shows on average a
 218 plateau over different bins.

219

220 **3.2 Machine learning predicts the stress fluctuations**

221 In order to establish the quantitative relation between microslips and the magnitude of global
 222 stress fluctuation, we resort to use the Extreme Gradient Boosting (XGBoost) technique to
 223 interrogate the data (Chen & Guestrin, 2016). Different from the Deep Learning, we need to
 224 extract physically reasonable features from the raw data for input for the Machine Learning (ML).
 225 The above analysis demonstrates a clear difference of microslips between recharge and drop
 226 events. Therefore, it is necessary to consider both the statistical and spatial characteristics of
 227 microslips in the feature extraction. We first calculate the maximum, mean, variance, skewness,
 228 and kurtosis of particle D_{min}^2 within each particle's second-neighbor shell (see Figure 3a),
 229 corresponding to the second minimum of pair correlation function shown in Figure S1a. These
 230 statistics contain information on how particle D_{min}^2 distributes in space. We then calculate the
 231 statistical features of each particle's medium range statistics (see Figure 3b). The statistical
 232 operator includes mean, max, variance, percentiles, and various higher-order moments. These
 233 statistical features are connected as the medium-range feature vector (MRF).

234

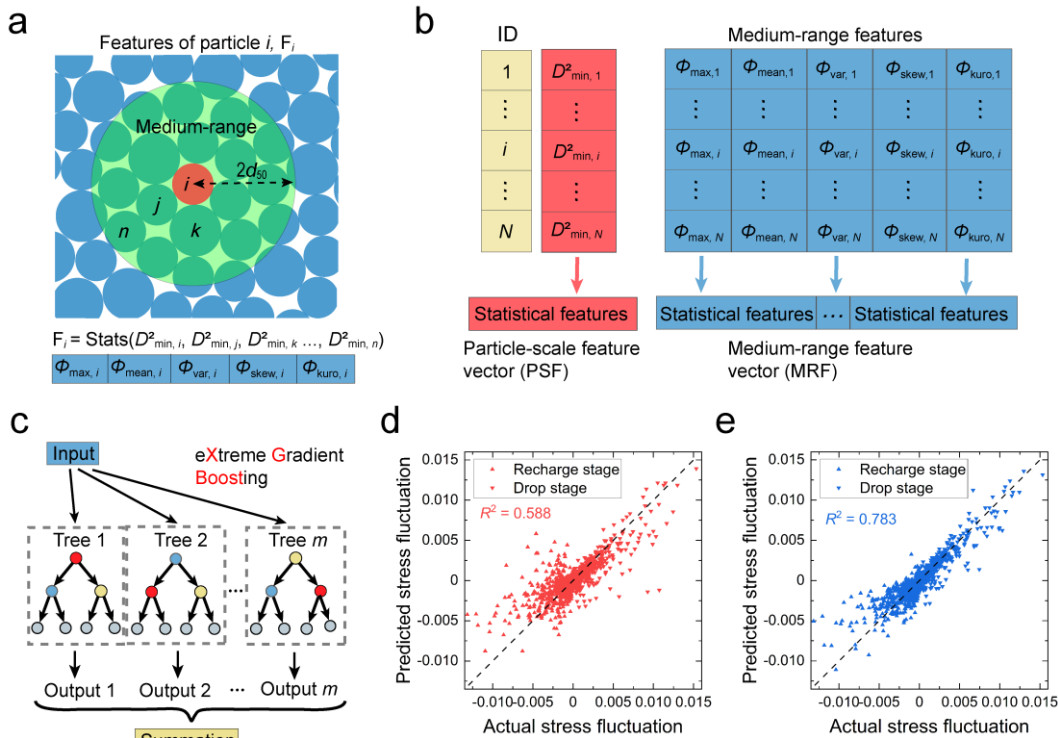
235 To highlight the importance of the spatial pattern of microslips in the prediction of global stress
 236 fluctuation, we also calculate the statistical features of particles D_{min}^2 as the input vector for
 237 XGBoost model training. This feature vector does not contain any information about the spatial
 238 distribution of microslips, and is referred to as particle-scale feature vector (PSF). MRF and PSF

239 are extracted for each recharge/drop event, and the corresponding output of XGBoost is the
 240 global stress fluctuation of the recharge/drop event. A typical structure of a XGBoost is depicted
 241 in Figure 3c. The XGBoost modeling process is briefly introduced in Text S3.

242

243 The shuffled dataset is divided into training set, test set, and validation set, with a proportion of
 244 60%, 20%, and 20%, respectively. The three sets do not overlap each other to avoid “information
 245 leakage”. The loss function of XGBoost for regression problems is the mean square error (MSE).
 246 The hyperparameters of XGBoost are tuned using Bayesian Optimization (Snoek et al., 2012).
 247 The performance of XGBoost models using PSF and MRF as inputs are shown in Figure 3d and
 248 Figure 3e, respectively. As can be seen, the trained XGBoost models not only classify the
 249 recharge and drop event from the microsliips, but also predict the magnitude of stress fluctuation
 250 with good accuracy. By taking into account both statistical and spatial characteristics of the
 251 microsliips, the trained XGBoost model exhibits better performance with a coefficient of
 252 determination $R^2 = 0.78$.

253



254 **Figure 3.** Machine learning builds the bridge between microsliips and global stress fluctuation. (a) The statistical
 255 characteristics of particle D_{\min}^2 within each particle’s second-neighbor shell. (b) Feature extraction process: particle-
 256 scale feature vector (red column) and medium-range feature vector (blue columns). These two feature vectors are
 257 fed as input to the downstream XGBoost model to predict global stress fluctuation. (c) Schematic of XGBoost (a
 258 supervised ML approach) based on the gradient boosting decision. Performance of XGBoost model trained by (d)
 259 PSF and (e) MRF, respectively.

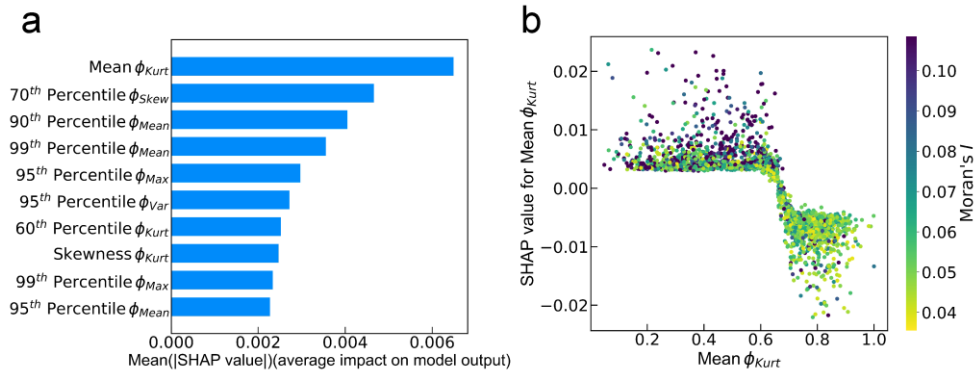
260

261
 262 Figure 3e depicts that certain success can be achieved in learning the complex relations between
 263 local and global avalanches for prediction. We further analyze the feature importance of the

264 XGBoost model trained by MRF. The feature importance is quantified by Shapley Additive
 265 Explanation (SHAP) value (Lundberg & Lee, 2017). The SHAP value for each feature is the
 266 average marginal contribution of a feature value across all possible coalitions, representing their
 267 contribution towards a higher or lower final prediction. Figure 4a shows the mean absolute
 268 SHAP values of the top 10 important features. The mean value of ϕ_{kurt} is the most important
 269 feature, changing the predicted absolute stress fluctuation on average by 0.6 percentage points.

270

271 ϕ_{kurt} measures the tail-heaviness of D_{min}^2 of a particle's second nearest neighbors (Westfall,
 272 2014). The smaller ϕ_{kurt} indicates the considered particle and its neighbors move in a corporative
 273 manner, i.e., particles with either high D_{min}^2 or low D_{min}^2 are spatially clustered. To investigate
 274 how the mean ϕ_{kurt} affects the model prediction, we present the SHAP dependence plot in Figure
 275 4b. Each dot denotes a recharge/drop event in the ML dataset, and the scatters are colored
 276 according to the global Moran's I of particle D_{min}^2 . The higher mean ϕ_{kurt} results in smaller and
 277 negative SHAP value, pushing the XGBoost prediction towards a recharge event. In contrast,
 278 microslips of a drop event demonstrate stronger spatial correlation and thus have smaller ϕ_{kurt} .
 279 This feature helps XGBoost to distinguish between the recharge and drop events and predict the
 280 magnitude of global stress fluctuation. This study reveals that the spatial distribution of
 281 microslips contains key information on the stress state of a granular gouge such that microslips
 282 (e.g., local acoustic emission signal and local seismic wave) detected inside the natural gouge
 283 faults may also serve useful to predict its frictional stability.



284

285 **Figure 4.** Feature importance analysis. (a) SHAP values for the top 10 important features. (b) Dependence plot for
 286 the mean value of ϕ_{kurt} , colored by the global moran's I .

287

288 4 Conclusions

289 We numerically investigated the relations between microslips and global stress fluctuation of a
 290 slowly sheared granular gouge. The microslip is manifested as irrisible particle rearrangement
 291 and is quantified by nonaffine particle motion. The statistical features and spatial distributions of
 292 microslips that occurred during the recharge and drop stages of a stick-slip cycle demonstrate
 293 apprantly different characteristics. Both the Moran's I and the correlation length of particle
 294 D_{min}^2 indicate that microslips in the drop stage are spatially correlated to form large local

295 avalanches, leading to large stress drop and frictional weakening. The difference in the
 296 microscopic dynamics of recharge and drop events suggest that we may quantitatively connect
 297 the microslips and global stress fluctuation.

298

299 The use of XGBoost boosts to build the bridge between microslips and macro stress fluctuation.
 300 Two sets of input fractures are extracted from the raw data to train the ML models. By using the
 301 input feature vector containing both statistical and spatial information of microslips, the trained
 302 XGBoost model can not only distinguish between recharge and drop events but also predict the
 303 magnitude of stress fluctuation with good accuracy. The feature importance analysis by SHAP
 304 values reveals that the kurtosis of D_{\min}^2 within each particle's first and second nearest neighbors
 305 is the most important feature, which characterize the local spatial autocorrelation of microslips.
 306 We conclude that the spatial distributions of microslips contain key information about the stress
 307 state of granular gouge fault and its frictional stability. It should be noted that there are many
 308 other ways to extract the spatial patterns of microslips, such as Convolutional Neural Network,
 309 Graph Embedding for feature extraction, and complex network analysis. This study may shed
 310 lights into the mechanisms governing earthquake nucleation, microslips, friction fluctuations,
 311 and their connection during the stick-slip dynamics of earthquake cycles.

312

313 **Acknowledgments, Samples, and Data**

314 We acknowledge the financial support from the National Natural Science Foundation of China
 315 (Grant No. 51825905, U1865204, and 51779194) and Science project of China Huaneng Group
 316 Co. Ltd (HNKJ18-H26). The numerical calculations in this work have been done on the
 317 supercomputing system in the Supercomputing Center of Wuhan University. The data supporting
 318 this paper can all be found at the corresponding author's figshare repository
 319 (https://figshare.com/articles/dataset/Machine_learning_bridges_microslips_and_slip_avalanches_of_sheared_granular_gouge/14099417).

321 **References**

- 322 Aharonov, E., & Sparks, D. (2004). Stick-slip motion in simulated granular layers. *Journal of Geophysical*
 323 *Research: Solid Earth*, *109*(9), 1–12. <https://doi.org/10.1029/2003JB002597>
- 324 Barés, J., Wang, D., Wang, D., Bertrand, T., O'Hern, C. S., & Behringer, R. P. (2017). Local and global avalanches
 325 in a two-dimensional sheared granular medium. *Physical Review E*, *96*(5), 1–13.
 326 <https://doi.org/10.1103/PhysRevE.96.052902>
- 327 Baró, J., Corral, Á., Illa, X., Planes, A., Salje, E. K. H., Schranz, W., et al. (2013). Statistical similarity between the
 328 compression of a porous material and earthquakes. *Physical Review Letters*, *110*(8), 1–5.
 329 <https://doi.org/10.1103/PhysRevLett.110.088702>
- 330 Bergen, K. J., Johnson, P. A., De Hoop, M. V., & Beroza, G. C. (2019). Machine learning for data-driven discovery
 331 in solid Earth geoscience. *Science*, *363*(6433). <https://doi.org/10.1126/science.aau0323>
- 332 Bolton, D. C., Marone, C., Shokouhi, P., Rivière, J., Rouet-Leduc, B., Hulbert, C., & Johnson, P. A. (2019).
 333 Characterizing acoustic signals and searching for precursors during the laboratory seismic cycle using
 334 unsupervised machine learning. *Seismological Research Letters*. <https://doi.org/10.1785/0220180367>
- 335 Bolton, D. C., Shreedharan, S., Rivière, J., & Marone, C. (2020). Acoustic Energy Release During the Laboratory
 336 Seismic Cycle: Insights on Laboratory Earthquake Precursors and Prediction. *Journal of Geophysical*
 337 *Research: Solid Earth*, *125*(8). <https://doi.org/10.1029/2019JB018975>
- 338 Byerlee, J. D., & Brace, W. F. (1966). Stick-Slip as a Mechanism for Earthquakes. *Science*, *153*(3739), 990–992.
- 339 Cao, P., Dahmen, K. A., Kushima, A., Wright, W. J., Park, H. S., Short, M. P., & Yip, S. (2018). Nanomechanics of

- 340 slip avalanches in amorphous plasticity. *Journal of the Mechanics and Physics of Solids*, 114, 158–171.
341 <https://doi.org/10.1016/j.jmps.2018.02.012>
- 342 Cao, P., Short, M. P., & Yip, S. (2019). Potential energy landscape activations governing plastic flows in glass
343 rheology. *Proceedings of the National Academy of Sciences of the United States of America*, 116(38), 18790–
344 18797. <https://doi.org/10.1073/pnas.1907317116>
- 345 Castellanos, D. F., & Zaiser, M. (2018). Avalanche Behavior in Creep Failure of Disordered Materials. *Physical*
346 *Review Letters*, 121(12), 125501. <https://doi.org/10.1103/PhysRevLett.121.125501>
- 347 Cipelletti, L., Martens, K., & Ramos, L. (2019). Microscopic precursors of failure in soft matter. *Soft Matter*, 16(1),
348 82–93. <https://doi.org/10.1039/c9sm01730e>
- 349 Corbi, F., Sandri, L., Bedford, J., Funicello, F., Brizzi, S., Rosenau, M., & Lallemand, S. (2019). Machine Learning
350 Can Predict the Timing and Size of Analog Earthquakes. *Geophysical Research Letters*, 46(3), 1303–1311.
351 <https://doi.org/10.1029/2018GL081251>
- 352 Denisov, D. V., Lörincz, K. A., Uhl, J. T., Dahmen, K. A., & Schall, P. (2016). Universality of slip avalanches in
353 flowing granular matter. *Nature Communications*, 7. <https://doi.org/10.1038/ncomms10641>
- 354 Dorostkar, O., & Carmeliet, J. (2018). Potential Energy as Metric for Understanding Stick–Slip Dynamics in
355 Sheared Granular Fault Gouge: A Coupled CFD–DEM Study. *Rock Mechanics and Rock Engineering*, 51(10),
356 3281–3294. <https://doi.org/10.1007/s00603-018-1457-6>
- 357 Dorostkar, O., & Carmeliet, J. (2019). Grain Friction Controls Characteristics of Seismic Cycle in Faults With
358 Granular Gouge. *Journal of Geophysical Research: Solid Earth*, 124(7), 6475–6489.
359 <https://doi.org/10.1029/2019JB017374>
- 360 Dorostkar, O., Guyer, R. A., Johnson, P. A., Marone, C., & Carmeliet, J. (2017a). On the micromechanics of slip
361 events in sheared, fluid-saturated fault gouge. *Geophysical Research Letters*, 44(12), 6101–6108.
362 <https://doi.org/10.1002/2017GL073768>
- 363 Dorostkar, O., Guyer, R. A., Johnson, P. A., Marone, C., & Carmeliet, J. (2017b). On the role of fluids in stick-slip
364 dynamics of saturated granular fault gouge using a coupled computational fluid dynamics-discrete element
365 approach. *Journal of Geophysical Research: Solid Earth*, 122(5), 3689–3700.
366 <https://doi.org/10.1002/2017JB014099>
- 367 Dorostkar, O., Guyer, R. A., Johnson, P. A., Marone, C., & Carmeliet, J. (2018). Cohesion-Induced Stabilization in
368 Stick-Slip Dynamics of Weakly Wet, Sheared Granular Fault Gouge. *Journal of Geophysical Research: Solid*
369 *Earth*, 123(3), 2115–2126. <https://doi.org/10.1002/2017JB015171>
- 370 Ferdowsi, B., Griffa, M., Guyer, R. A., Johnson, P. A., Marone, C., & Carmeliet, J. (2013). Microslips as precursors
371 of large slip events in the stick-slip dynamics of sheared granular layers: A discrete element model analysis.
372 *Geophysical Research Letters*, 40(16), 4194–4198. <https://doi.org/10.1002/grl.50813>
- 373 Ferdowsi, B., Griffa, M., Guyer, R. A., Johnson, P. A., & Carmeliet, J. (2014a). Effect of boundary vibration on the
374 frictional behavior of a dense sheared granular layer. *Acta Mechanica*, 225(8), 2227–2237.
375 <https://doi.org/10.1007/s00707-014-1136-y>
- 376 Ferdowsi, B., Griffa, M., Guyer, R. A., Johnson, P. A., Marone, C., & Carmeliet, J. (2014b). Three-dimensional
377 discrete element modeling of triggered slip in sheared granular media. *Physical Review E - Statistical,*
378 *Nonlinear, and Soft Matter Physics*, 89(4), 1–12. <https://doi.org/10.1103/PhysRevE.89.042204>
- 379 Ferdowsi, B., Griffa, M., Guyer, R. A., Johnson, P. A., Marone, C., & Carmeliet, J. (2015). Acoustically induced
380 slip in sheared granular layers: Application to dynamic earthquake triggering. *Geophysical Research Letters*,
381 42(22), 9750–9757. <https://doi.org/10.1002/2015GL066096>
- 382 Gao, K., Euser, B. J., Rougier, E., Guyer, R. A., Lei, Z., Knight, E. E., et al. (2018). Modeling of Stick-Slip
383 Behavior in Sheared Granular Fault Gouge Using the Combined Finite-Discrete Element Method. *Journal of*
384 *Geophysical Research: Solid Earth*. <https://doi.org/10.1029/2018JB015668>
- 385 Gao, K., Guyer, R., Rougier, E., Ren, C. X., & Johnson, P. A. (2019). From Stress Chains to Acoustic Emission.
386 *Physical Review Letters*, 123(4). <https://doi.org/10.1103/PhysRevLett.123.048003>
- 387 Hulbert, C., Rouet-Leduc, B., Johnson, P. A., Ren, C. X., Rivière, J., Bolton, D. C., & Marone, C. (2019). Similarity
388 of fast and slow earthquakes illuminated by machine learning. *Nature Geoscience*, 12(1), 69–74.
389 <https://doi.org/10.1038/s41561-018-0272-8>
- 390 Johnson, P. A., Ferdowsi, B., Kaproth, B. M., Scuderi, M., Griffa, M., Carmeliet, J., et al. (2013). Acoustic emission
391 and microslip precursors to stick-slip failure in sheared granular material. *Geophysical Research Letters*,
392 40(21), 5627–5631. <https://doi.org/10.1002/2013GL057848>
- 393 Kloss, C., Goniva, C., Hager, A., Amberger, S., & Pirker, S. (2012). Models , algorithms and validation for
394 opensource DEM and CFD-DEM. *Progress in Computational Fluid Dynamics*, 12(2–3), 140–152.
- 395 Leeman, J. R., Saffer, D. M., Scuderi, M. M., & Marone, C. (2016). Laboratory observations of slow earthquakes

- 396 and the spectrum of tectonic fault slip modes. *Nature Communications*, 7, 1–6.
397 <https://doi.org/10.1038/ncomms11104>
- 398 Liu, J., Wautier, A., Bonelli, S., Nicot, F., & Darve, F. (2020). Macroscopic softening in granular materials from a
399 mesoscale perspective. *International Journal of Solids and Structures*, 193–194, 222–238.
400 <https://doi.org/10.1016/j.ijsolstr.2020.02.022>
- 401 Lundberg, S. M., & Lee, S. I. (2017). A unified approach to interpreting model predictions. *Advances in Neural
402 Information Processing Systems* 30, 4765–4774.
- 403 Ma, G., Regueiro, R. A., Zhou, W., Wang, Q., & Liu, J. (2018). Role of particle crushing on particle kinematics and
404 shear banding in granular materials. *Acta Geotechnica*, 13(3), 601–618. <https://doi.org/10.1007/s11440-017-0621-6>
- 405
- 406 Ma, G., Regueiro, R. A., Zhou, W., & Liu, J. (2019). Spatiotemporal analysis of strain localization in dense granular
407 materials. *Acta Geotechnica*, 14(4), 973–990. <https://doi.org/10.1007/s11440-018-0685-y>
- 408 Ma, G., Zou, Y., Gao, K., Zhao, J., & Zhou, W. (2020). Size Polydispersity Tunes Slip Avalanches of Granular
409 Gouge. *Geophysical Research Letters*, 47(23), 1–9. <https://doi.org/10.1029/2020gl090458>
- 410 Ma, G., Zou, Y., Chen, Y., Tang, L., Ng, T. T., & Zhou, W. (2021). Spatial correlation and temporal evolution of
411 plastic heterogeneity in sheared granular materials. *Powder Technology*.
412 <https://doi.org/10.1016/j.powtec.2020.09.053>
- 413 Mair, K., & Hazzard, J. F. (2007). Nature of stress accommodation in sheared granular material: Insights from 3D
414 numerical modeling. *Earth and Planetary Science Letters*, 259(3–4), 469–485.
415 <https://doi.org/10.1016/j.epsl.2007.05.006>
- 416 Mair, K., Frye, K. M., & Marone, C. (2002). Influence of grain characteristics on the friction of granular shear
417 zones. *Journal of Geophysical Research: Solid Earth*, 107(B10), ECV 4-1-ECV 4-9.
418 <https://doi.org/10.1029/2001jb000516>
- 419 Marone, C. (1998). The effect of loading rate on static friction and the rate of fault healing during the earthquake
420 cycle. *Nature*, 391(6662), 69–72. <https://doi.org/10.1038/34157>
- 421 Marone, C. (2018). Training machines in Earthly ways. *Nature Geoscience*, 11(5), 301–302.
422 <https://doi.org/10.1038/s41561-018-0117-5>
- 423 Marone, C., Scholtz, C. H., & Bilham, R. (1991). On the mechanics of earthquake afterslip. *Journal of Geophysical
424 Research*, 96(B5), 8441–8452. <https://doi.org/10.1029/91JB00275>
- 425 Mousavi, S. M., & Beroza, G. C. (2020). A Machine-Learning Approach for Earthquake Magnitude Estimation.
426 *Geophysical Research Letters*, 47(1), 1–7. <https://doi.org/10.1029/2019GL085976>
- 427 Mousavi, S. M., Ellsworth, W. L., Zhu, W., Chuang, L. Y., & Beroza, G. C. (2020). Earthquake transformer—an
428 attentive deep-learning model for simultaneous earthquake detection and phase picking. *Nature
429 Communications*, 11(1), 1–12. <https://doi.org/10.1038/s41467-020-17591-w>
- 430 Nanjo, K. Z. (2020). Were changes in stress state responsible for the 2019 Ridgecrest, California, earthquakes?
431 *Nature Communications*, 11(1), 3–6. <https://doi.org/10.1038/s41467-020-16867-5>
- 432 Niemeijer, A., Marone, C., & Elsworth, D. (2010). Frictional strength and strain weakening in simulated fault
433 gouge: Competition between geometrical weakening and chemical strengthening. *Journal of Geophysical
434 Research: Solid Earth*, 115(10), 1–16. <https://doi.org/10.1029/2009JB000838>
- 435 Rathbun, A. P., Renard, F., & Abe, S. (2013). Numerical investigation of the interplay between wall geometry and
436 friction in granular fault gouge. *Journal of Geophysical Research: Solid Earth*, 118(3), 878–896.
437 <https://doi.org/10.1002/jgrb.50106>
- 438 Ren, C. X., Dorostkar, O., Rouet-Leduc, B., Hulbert, C., Strelbel, D., Guyer, R. A., et al. (2019). Machine Learning
439 Reveals the State of Intermittent Frictional Dynamics in a Sheared Granular Fault. *Geophysical Research
440 Letters*, 46(13), 7395–7403. <https://doi.org/10.1029/2019GL082706>
- 441 Ren, C. X., Hulbert, C., Johnson, P. A., & Rouet-Leduc, B. (2020). Machine learning and fault rupture: A review.
442 *Advances in Geophysics*, 61, 57–107. <https://doi.org/10.1016/bs.agph.2020.08.003>
- 443 Rivière, J., Lv, Z., Johnson, P. A., & Marone, C. (2018). Evolution of b-value during the seismic cycle: Insights
444 from laboratory experiments on simulated faults. *Earth and Planetary Science Letters*, 482, 407–413.
445 <https://doi.org/10.1016/j.epsl.2017.11.036>
- 446 Rouet-Leduc, B., Hulbert, C., Lubbers, N., Barros, K., Humphreys, C. J., & Johnson, P. A. (2017). Machine
447 Learning Predicts Laboratory Earthquakes. *Geophysical Research Letters*, 44(18), 9276–9282.
448 <https://doi.org/10.1002/2017GL074677>
- 449 Rouet-Leduc, B., Hulbert, C., Bolton, D. C., Ren, C. X., Riviere, J., Marone, C., et al. (2018). Estimating Fault
450 Friction From Seismic Signals in the Laboratory. *Geophysical Research Letters*, 45(3), 1321–1329.
451 <https://doi.org/10.1002/2017GL076708>

- 452 Rouet-Leduc, B., Hulbert, C., & Johnson, P. A. (2019). Continuous chatter of the Cascadia subduction zone revealed
453 by machine learning. *Nature Geoscience*, *12*(1), 75–79. <https://doi.org/10.1038/s41561-018-0274-6>
- 454 Scuderi, M. M., Carpenter, B. M., Johnson, P. A., & Marone, C. (2015). Poromechanics of stick-slip frictional
455 sliding and strength recovery on tectonic faults. *Journal of Geophysical Research: Solid Earth*, *120*(10),
456 6895–6912. <https://doi.org/10.1002/2015JB011983>.
- 457 Scuderi, M. M., Marone, C., Tinti, E., Di Stefano, G., & Collettini, C. (2016). Precursory changes in seismic
458 velocity for the spectrum of earthquake failure modes. *Nature Geoscience*, *9*(9), 695–700.
459 <https://doi.org/10.1038/ngeo2775>
- 460 Snoek, J., Larochelle, H., & Adams, R. P. (2012). Practical Bayesian Optimization of Machine Learning
461 Algorithms. *Proceedings of the 25th International Conference on Neural Information Processing Systems*, *25*,
462 2951–2959.
- 463 Song, D., Ng, C. W. W., Choi, C. E., Zhou, G. G. D., Kwan, J. S. H., & Koo, R. C. H. (2017). Influence of debris
464 flow solid fraction on rigid barrier impact. *Canadian Geotechnical Journal*, *54*(10), 1421–1434.
465 <https://doi.org/10.1139/cgj-2016-0502>
- 466 Sun, B. A., Pauly, S., Tan, J., Stoica, M., Wang, W. H., Kühn, U., & Eckert, J. (2012). Serrated flow and stick-slip
467 deformation dynamics in the presence of shear-band interactions for a Zr-based metallic glass. *Acta*
468 *Materialia*, *60*(10), 4160–4171. <https://doi.org/10.1016/j.actamat.2012.04.013>
- 469 Chen, T., & Guestrin, C. (2016). XGBoost: A Scalable Tree Boosting System. *The Journal of the Association of*
470 *Physicians of India*, *42*(8), 665.
- 471 Tinti, E., Scuderi, M. M., Scognamiglio, L., Di Stefano, G., Marone, C., & Collettini, C. (2016). On the evolution of
472 elastic properties during laboratory stick-slip experiments spanning the transition from slow slip to dynamic
473 rupture. *Journal of Geophysical Research: Solid Earth*, *121*(12), 8569–8594.
474 <https://doi.org/10.1002/2016JB013545>
- 475 Trugman, D. T., McBrearty, I. W., Bolton, D. C., Robert, A., Marone, C., & Johnson, P. A. (2020). The Spatio-
476 temporal Evolution of Granular Microslip Precursors to Laboratory Earthquakes. *Geophysical Research*
477 *Letters*, 1–10. <https://doi.org/10.1029/2020GL088404>
- 478 Wang, D., Carmeliet, J., Zhou, W., & Dorostkar, O. (2020). On the effect of grain fragmentation on frictional
479 instabilities in faults with granular gouge. EarthArxiv.
- 480 Westfall, P. H. (2014). Kurtosis as Peakedness, 1905–2014. R.I.P. *American Statistician*, *68*(3), 191–195.
481 <https://doi.org/10.1080/00031305.2014.917055>
- 482 Zheng, J., Sun, A., Wang, Y., & Zhang, J. (2018). Energy Fluctuations in Slowly Sheared Granular Materials.
483 *Physical Review Letters*, *121*(24), 248001. <https://doi.org/10.1103/PhysRevLett.121.248001>
- 484